


SCIENTIFIC REPORTS



OPEN

Cellular toxicity pathways of inorganic and methyl mercury in the green microalga *Chlamydomonas reinhardtii*

Rebecca Beauvais-Flück, Vera I. Slaveykova & Claudia Cosio 

Contamination by mercury (Hg) is a worldwide concern because of Hg toxicity and biomagnification in aquatic food webs. Nevertheless, bioavailability and cellular toxicity pathways of inorganic (IHg) and methyl-Hg (MeHg) remain poorly understood. We analyzed the uptake, transcriptomic, and physiological responses in the microalga *Chlamydomonas reinhardtii* exposed to IHg or MeHg. Bioavailability of MeHg was up to $27 \times$ higher than for IHg. Genes involved in cell processes, energy metabolism and transport were dysregulated by both Hg species. Physiological analysis revealed an impact on photosynthesis and reduction–oxidation reaction metabolism. Nevertheless, MeHg dysregulated a larger number of genes and with a stronger fold-change than IHg at equivalent intracellular concentration. Analysis of the perturbations of the cell's functions helped to derive a detailed mechanistic understanding of differences in cellular handling of IHg and MeHg resulting in MeHg having a stronger impact. This knowledge is central for the prediction of impact of toxicants on organisms.

Widespread mercury (Hg) contamination of aquatic environment leads to accumulation of high levels of Hg in organisms and can have a detrimental effect on biota and humans^{1–5}. Exposure of primary producers such as phytoplankton to low concentrations of inorganic Hg (Hg^{2+} , IHg) and methyl-Hg (CH_3Hg^+ , MeHg) can threaten the aquatic systems functioning^{6,7}. IHg and MeHg exist in different forms, i.e. free uncomplexed ion, bound to natural ligands, particles and colloids, each with different reactivity, biological availability and toxicity in biota^{7,8}. There is substantial evidence that exposure to both IHg and MeHg induces general toxic effects in primary producers including reduction of growth and photosynthesis as well as oxidative stress (see refs 6 and 7 for review). Nevertheless, differences between the fate and the toxicity of IHg and MeHg in organisms have been observed^{9–11}. Field studies have shown higher uptake of MeHg than IHg, as well as exclusive biomagnification of MeHg in the food chain⁹. Exposure to IHg increased the lifetime of chlorophyll fluorescence by blocking the photosynthetic electron chain in the marine diatom *Thalassiosira weissflogii* while MeHg had no significant effect¹⁰. IHg affected the plasma membrane integrity whereas MeHg disturbs organelle metabolism in the cytoplasm, subsequently affecting membrane integrity¹¹. It was recently shown that sub-nanomolar concentrations of MeHg significantly altered the energy metabolism (photosynthesis and sugars) and the antioxidant activity of the green microalga *Chlamydomonas reinhardtii*¹². However, most of these evidences were obtained in studies conducted at 10^3 to 10^6 higher Hg concentrations than those typically found in natural water and so limiting their environmental relevance. Furthermore, the above reported Hg-induced effects are classically assessed by examining the growth, or physiology perturbation of organism but these parameters fall short of revealing subtle effects occurring prior changes at the organism level and tolerance responses that allow the organism to adapt and recover at environmental concentrations. Consequently, little is known about both the impact of IHg and MeHg on microalgae at low environmental Hg concentrations and the possible cellular toxicity pathways of IHg and MeHg in aquatic primary producers.

Environmental Biogeochemistry and Ecotoxicology, Department F.-A. Forel for environmental and aquatic sciences, Earth and Environmental Sciences, Faculty of Sciences, University of Geneva, 66, boulevard Carl-Vogt, 1211, Geneva 4, Switzerland. Correspondence and requests for materials should be addressed to C.C. (email: Claudia.Cosio@unige.ch)

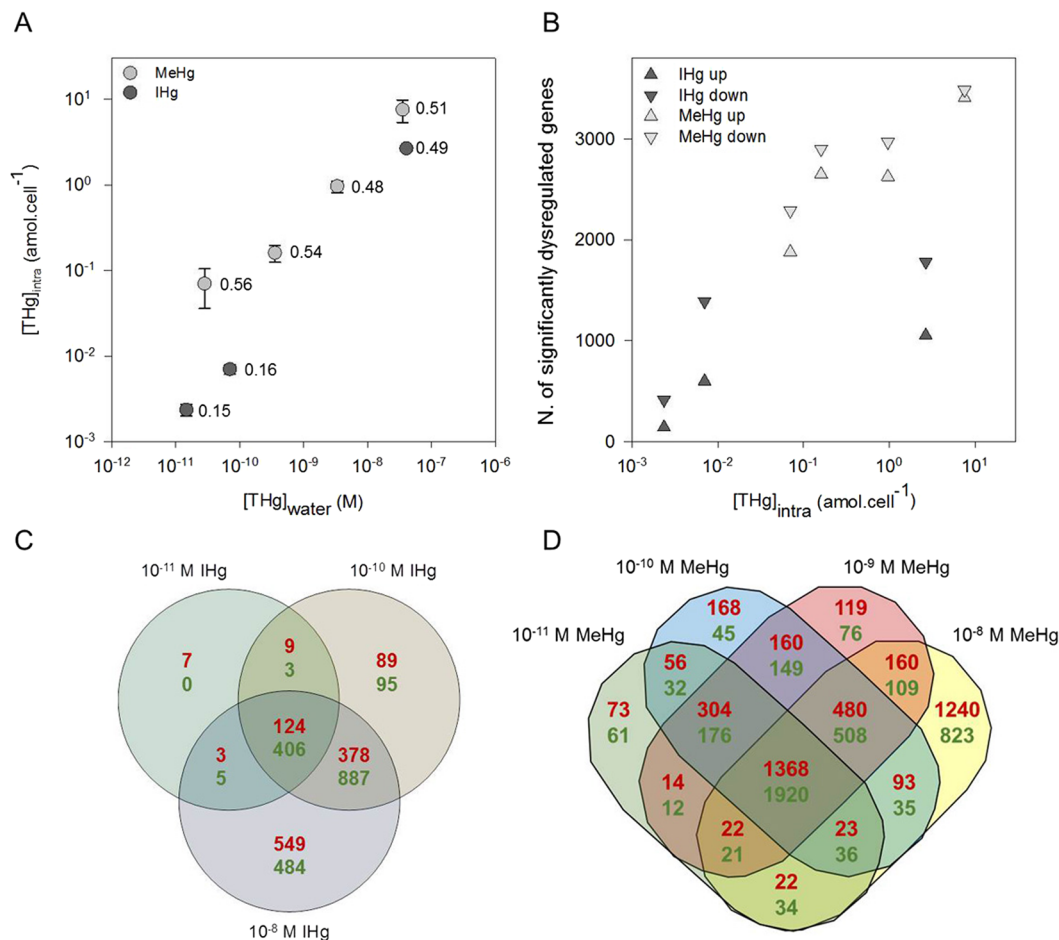


Figure 1. Intracellular total Hg concentrations ($[\text{THg}]_{\text{intra}}$, mean \pm sd, $n = 3$) in *C. reinhardtii* exposed to IHg or MeHg, as a function of initial IHg or MeHg exposure concentration expressed as THg ($[\text{THg}]_{\text{water}}$). Values indicate ratio of $[\text{THg}]_{\text{intra}}$ to $[\text{THg}]_{\text{intra+ads}}$, lines show linear regressions of \log_{10} values (A). Number of significantly up- and down-regulated genes (EdgeR FDR < 0.1%) as a function of $[\text{THg}]_{\text{intra}}$ (B). Venn diagrams showing the number of up- (red, upper numbers) and down- (green, lower numbers) significantly regulated genes in *C. reinhardtii* after 2 h exposure to IHg (C) or MeHg (D) (EdgeR, FDR < 0.1%).

In this context, transcriptomics (e.g. RNA-Sequencing; RNA-Seq) is considered to be a powerful tool for early detection of adverse outcome pathways as well as tolerance response¹³, notably when analyzed concomitantly with other endpoints¹⁴. By following the transcriptomic and physiological responses in parallel with cellular Hg concentrations, the comparative study presented here aims to explore the influence of a range of IHg and MeHg concentrations below and above the European environmental quality standard for Hg ($2.5 \cdot 10^{-9}$ M)¹⁵ on the green alga *C. reinhardtii*. The following key questions were addressed: (i) What are the cellular toxicity pathways in *C. reinhardtii* exposed to IHg and MeHg? (ii) How similar or different are they for IHg and MeHg? More in details, the effects of IHg and MeHg on the microalga *C. reinhardtii* were assessed by studying the dysregulation of gene expression, the generation of intracellular reactive oxygen species (ROS), and the photosynthesis efficiency at the physiological level, and by exploring the link with the intracellular concentrations of IHg and MeHg, used as a measure of Hg species bioavailability.

Results and Discussion

IHg and MeHg bioavailability to *C. reinhardtii*. Speciation modelling of IHg and MeHg in the exposure medium revealed that neutral hydroxo- (-OH) and chloro- (-Cl) complexes were predominant for both IHg and MeHg (Figure S1). The cation CH_3Hg^+ represented 0.3% of the total MeHg in the medium. The most abundant IHg cation, HgCl^+ reached $6 \cdot 10^{-3}\%$, while the free ion Hg^{2+} concentrations represented only $1 \cdot 10^{-6}\%$ of the total IHg (Figure S1). These results suggest that the processes at medium-alga interface determining bioavailability may involve different predominant species in IHg and MeHg exposure^{7,8}. Nevertheless, although multicomponent thermodynamic equilibrium speciation modeling is widely used and highly informative, it also involves significant uncertainties due to the model assumptions and available stability constants¹⁶.

Bioavailability of IHg and MeHg in the different treatments was then determined by measuring intracellular $[\text{THg}]_{\text{intra}}$ and whole cell $[\text{THg}]_{\text{intra+ads}}$ concentrations. At 10^{-11} and 10^{-10} M IHg, $[\text{THg}]_{\text{intra}}$ represented $16 \pm 1\%$ of $[\text{THg}]_{\text{intra+ads}}$ (Fig. 1A, Table S1), suggesting that the most part of Hg was loosely bound to the algal surface

| Metabolic Pathways | Number of genes | | | | | | |
|-----------------------|-----------------------|-------------------|------------------|------------------------|-------------------|------------------|------------------|
| | IHg concentration (M) | | | MeHg concentration (M) | | | |
| | 10 ⁻¹¹ | 10 ⁻¹⁰ | 10 ⁻⁸ | 10 ⁻¹¹ | 10 ⁻¹⁰ | 10 ⁻⁹ | 10 ⁻⁸ |
| Amino acid metabolism | 1 | 10 | 17 | 31 | 45 | 45 | 69 |
| Cell processes | 68 | 455 | 505 | 611 | 668 | 665 | 746 |
| Energy metabolism | 23 | 60 | 83 | 110 | 125 | 127 | 250 |
| Gene expression | 90 | 295 | 452 | 714 | 941 | 942 | 1173 |
| Lipid metabolism | 2 | 13 | 18 | 42 | 59 | 62 | 78 |
| Other metabolisms | 9 | 32 | 53 | 83 | 123 | 130 | 158 |
| RedOx | 0 | 7 | 9 | 18 | 24 | 24 | 34 |
| Signaling | 7 | 24 | 38 | 54 | 66 | 68 | 87 |
| Stress | 5 | 11 | 14 | 24 | 34 | 39 | 43 |
| Transport | 24 | 70 | 87 | 141 | 165 | 168 | 218 |

Table 1. Number of significantly dysregulated genes in metabolic pathways (MapMan) in *C. reinhardtii* after 2 h exposure to increasing concentrations of IHg and MeHg (numbers in bold show categories with high dysregulation according to Wilcoxon test, $p < 0.05$).

and extractable by molecules with strong affinity for Hg (i.e. cysteine). This ratio at all tested concentrations of MeHg was about $3.3 \times$ larger ($53 \pm 12\%$; Fig. 1A, Table S1), suggesting different fate for IHg and MeHg forms in *C. reinhardtii*. Indeed, no measurable demethylation of MeHg in the media or during uptake in *C. reinhardtii* was found. In fact, 100% of all $[\text{THg}]_{\text{water}}$ were in the form of MeHg in MeHg treatments. Similarly, 100% of $[\text{THg}]_{\text{intra}}$ were in the form of MeHg except at 10^{-11} M MeHg concentration where MeHg represented 30% of $[\text{THg}]_{\text{intra}}$ due to the IHg background concentration in the algae. Furthermore, $[\text{THg}]_{\text{intra}}$ increased linearly with the initial Hg concentration in exposure medium $[\text{THg}]_{\text{water}}$ (IHg: $n = 3$, $R^2 = 0.996 \pm 0.101$, $p = 0.03$; MeHg: $n = 4$, $R^2 = 0.941 \pm 0.218$, $p = 0.02$; Fig. 1A, Table S1). At comparable exposure concentrations of 10^{-11} and 10^{-8} M IHg and MeHg, $[\text{THg}]_{\text{intra}}$ was respectively $27 \times$ and $3 \times$ higher for MeHg exposure than for IHg exposure. These observations are in line with the results of field studies showing a $2 \times$ to $4 \times$ higher bioaccumulation of MeHg than IHg^{6,9}. However, they differ from the comparable intracellular contents of ¹⁹⁹IHg and ²⁰¹MeHg found in the 48 h exposure to their mixtures in the range 10^{-12} – 10^{-9} M¹⁷. The shorter exposure duration used here and the different exposure medium that affect speciation, and so Hg bioavailability, may explain this dissimilarity. Indeed, it is well established that speciation affects uptake, although Hg uptake pathways are still unclear¹². Simple passive diffusion was proposed for small neutral lipophilic complexes (i.e. HgCl_2^0 , and MeHgCl^0) while uptake by carrier-mediated transport has also been demonstrated for other complexes^{18–22}.

Global changes in gene expression in response to IHg and MeHg. The number of reads ranged from 18.7 to $22.6 \cdot 10^6$, with an average mapping of 86.2% (Table S2). Altogether, 8461 genes were dysregulated by Hg treatments, representing 47.7% of the total number of genes in *C. reinhardtii* genome. The numbers of down-regulated genes for both IHg and MeHg were larger than the up-regulated genes, except at 10^{-8} M MeHg (Fig. 1B, Tables S2 and S3). The number of dysregulated genes increased at higher $[\text{THg}]_{\text{intra}}$ for both IHg and MeHg exposure. Furthermore, for comparable $[\text{THg}]_{\text{intra}}$, MeHg induced dysregulation of a larger number of genes than IHg showing that MeHg induced a stronger molecular response in the cell. For example, at $1 \text{ amol}_{\text{THg}} \cdot \text{cell}^{-1}$, $4.4 \times$ more genes were up-regulated by MeHg than IHg (Fig. 1B). Moreover, 15.7% of dysregulated genes had a fold change >4 or <-4 at 10^{-8} M MeHg concentration, while this percentage represented 0.4 to 6.7%, for 10^{-11} M IHg to 10^{-9} M MeHg, suggesting that the exposure to the higher concentration of MeHg resulted in a stronger molecular impact than other treatments. In addition, dysregulated genes specific to IHg represented only 4% (133) of all IHg regulated genes (3038), whereas 65% (5423) of MeHg affected genes (8328) were specific to MeHg (Fig. 1C,D). In summary, for comparable exposure concentration, greater uptake of MeHg than IHg was observed and for equivalent $[\text{THg}]_{\text{intra}}$ a larger number of dysregulated genes for MeHg than IHg exposure were found. These observations support a different fate at the subcellular level of IHg and MeHg at similar exposure concentration.

Metabolic pathways involved in *C. reinhardtii* transcriptomic and physiological response to IHg and MeHg. Although the “intensity” of the response was stronger at MeHg exposure, gene ontology (GO) of the differentially dysregulated genes showed that similar biological pathways were altered by both IHg and MeHg. These are pathways involved in regulation of gene expression (nucleotide to protein synthesis, signaling), cell processes (motility, division, development), energy metabolism (photosynthesis, sugar metabolism), lipid metabolism, amino acid metabolism, stress and transport, providing indications on cellular targets in *C. reinhardtii* (Table 1, Fig. 2, Figures S2 and S3, Tables S3 and S4).

The number of dysregulated genes in all these categories increased from $2.8 \times$ to $17 \times$ for exposure to IHg from 10^{-11} to 10^{-8} M, and from $1.2 \times$ to $2.3 \times$ for exposure to MeHg from 10^{-11} to 10^{-8} M. The increasing number of dysregulated genes in the different categories was congruent with the increase of $[\text{THg}]_{\text{intra}}$ measured for IHg or MeHg exposure and highlights the tolerance response of the microalga to tolerate increasing $[\text{THg}]_{\text{intra}}$ (Figure S4). Interestingly, for similar $[\text{THg}]_{\text{intra}}$, exposure to MeHg dysregulated $1.3 \times$ to $4.1 \times$ more genes in these categories than IHg exposures (Figure S4), supporting a greater impact on the cellular machinery of MeHg.

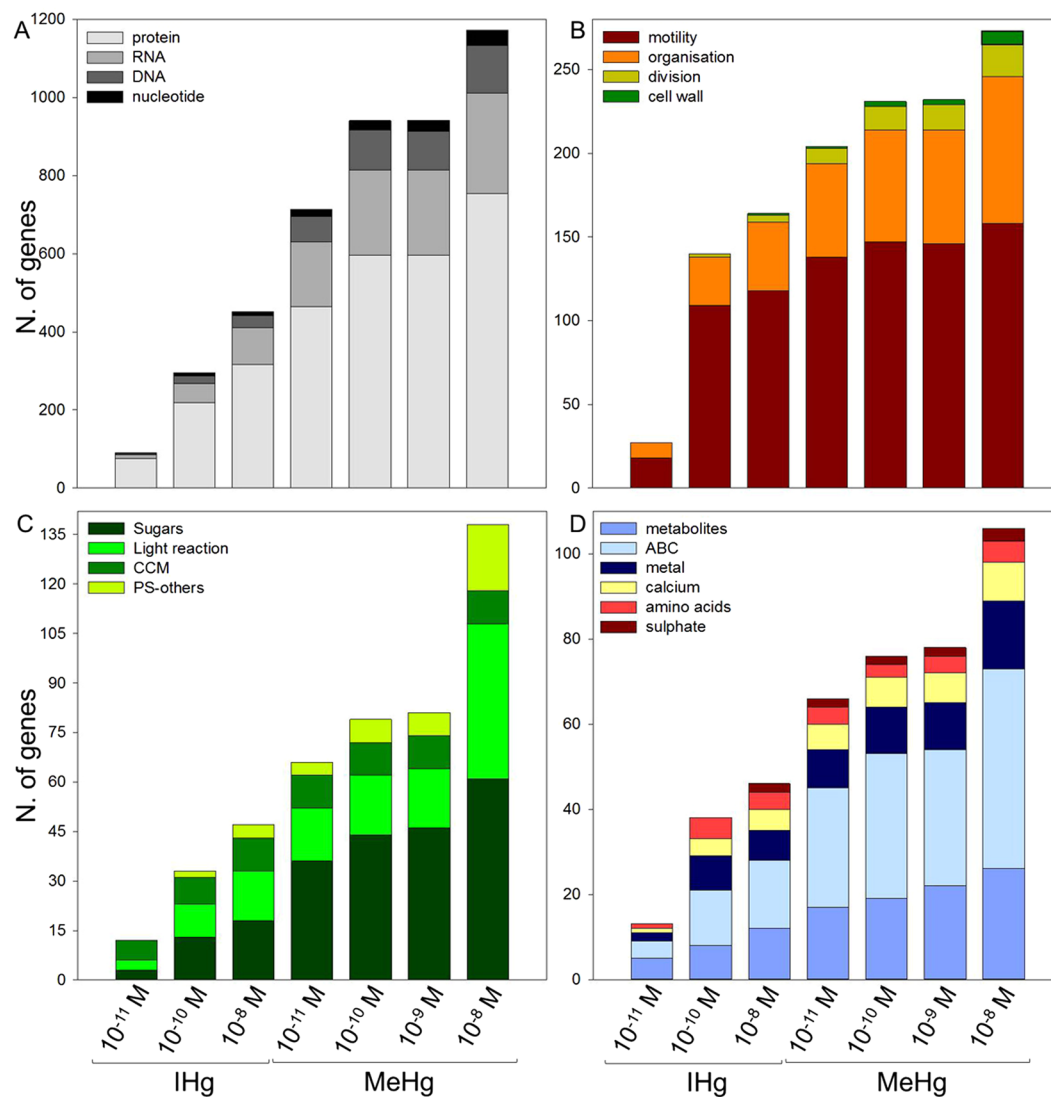


Figure 2. Number of genes significantly dysregulated in *C. reinhardtii* after 2 h exposure to increasing concentrations of IHg or MeHg (MapMan) in the categories involved in gene expression (A), cell processes (B), energy metabolism (C) and transport (D).

Furthermore, these observations support a different subcellular fate for MeHg and IHg. The main dysregulated categories and the clues they give on subcellular targets of IHg and MeHg are discussed below.

Cell processes: motility, organization, division, and cell wall. Dysregulated genes involved in cellular processes, notably the cell motility and cell organization categories, were among the most strongly affected during exposure to both IHg and MeHg (Table 1, Table S4). Genes involved in the cell motility showed a strong response at all concentrations. More specifically, 10 genes coding for flagellar associated proteins were already strongly down-regulated at 10^{-11} M IHg and the number of regulated genes further increased in the other treatments (27 and 36 down-regulated genes for 10^{-10} and 10^{-8} M IHg, respectively, and up to 44 down-regulated and 4 up-regulated genes at 10^{-8} M MeHg). The regulation of the expression of genes related to flagella supports a possible impact of Hg on *C. reinhardtii* motility, as reported for other metals and MeHg in microalgae^{12,23}. Here, several genes involved in the cell division were also dysregulated. In particular, the gene coding for HORMA Mitotic spindle assembly checkpoint protein was down-regulated in 10^{-10} and 10^{-9} M MeHg and 10^{-10} and 10^{-8} M IHg treatments while other transcripts in this category were up-regulated. Genes involved in the cell wall metabolism and lignin biosynthesis (phenylpropanoids), notably glycoproteins (e.g. Cre16.g668850.t1.3, hydroxyproline-rich glycoprotein, \log_2FC -0.79 , FDR $5.61 \cdot 10^{-7}$) and expansin (Cre08.g381600.t1.2, expansin A24, \log_2FC 2.71, FDR $8.88 \cdot 10^{-5}$) were only up-regulated at 10^{-8} M MeHg concentration. Similarly, expansin was strongly up-regulated by salt stress subsequently inducing the formation of palmelloids in *C. reinhardtii* and therefore it has been hypothesized that it is involved in the extension of cell walls during cell division to tolerate stress²⁴. Here, genes involved in the cell organization were also strongly dysregulated. For example, the expression of fibrillin (e.g. Cre14.g618050.t1.2, plastid-lipid associated protein PAP/fibrillin) was up-regulated in all treatments except at

| | Treatment | Cells with affected membrane permeability (%) | Cells with increased intracellular ROS (%) | [chl <i>a</i>] (% of control) | F _v /F _m (% of control) |
|------|---------------------|---|--|--------------------------------|---|
| IHg | Control | 17.7 ± 3.4 | 12.0 ± 1.5 | 100.0 ± 0.6 | 100.0 ± 1.7 |
| | 10 ⁻¹¹ M | 14.9 ± 0.1 | 11.2 ± 1.3 | 106.4 ± 5.9 | 107.2 ± 0.2 |
| | 10 ⁻¹⁰ M | 16.8 ± 2.6 | 11.6 ± 3.5 | 110.5 ± 5.6 | 110.8 ± 0.9 |
| | 10 ⁻⁸ M | 21.5 ± 2.1 | 12.3 ± 1.6 | 99.5 ± 4.9 | 103.2 ± 0.6 |
| MeHg | Control | 17.7 ± 3.4 | 12.0 ± 1.5 | 100.0 ± 11.2 | 100.0 ± 1.6 |
| | 10 ⁻¹¹ M | 24.6 ± 6.4 | 14.9 ± 0.4 | 95.0 ± 1.0 | 123.0 ± 1.8 |
| | 10 ⁻¹⁰ M | 24.4 ± 3.9 | 16.3 ± 2.3 | 101.7 ± 3.1 | 125.0 ± 0.4 |
| | 10 ⁻⁹ M | 23.6 ± 1.6 | 15.0 ± 1.0 | 93.4 ± 18.9 | 130.3 ± 1.9 |
| | 10 ⁻⁸ M | 18.5 ± 3.3 | 14.9 ± 0.9 | 78.8 ± 15.1 | 115.6 ± 1.5 |

Table 2. Effects of IHg and MeHg on physiological endpoints in *C. reinhardtii* after 2 h exposure (bold characters indicate significantly different result from the control; t-test *p*-value < 0.05).

the 10⁻¹¹ M IHg concentration. Fibrillin is part of the plastoglobule proteome²⁵, suggesting an impact of IHg and MeHg exposure on the synthesis of reserve lipid bodies. Overall, the results demonstrate that genes involved in the development and motility of *C. reinhardtii* were affected by IHg and MeHg at all the concentrations tested.

Energy metabolism. Genes involved in the carbon concentrating mechanism (CCM) were strongly dysregulated in *C. reinhardtii* by both IHg and MeHg (Tables S3 and S4), which is in agreement with previous studies suggesting that carbon acquisition could be impacted by MeHg in *C. reinhardtii*^{12,26}. For instance, LCIB, a gene involved in inorganic carbon (C) accumulation in the chloroplast²⁷, was strongly up-regulated (Cre04.g223250.t1.3, log₂FC 2.19 and FDR 5.12·10⁻⁴ for 10⁻⁸ M IHg, log₂FC 2.68 and FDR 1.87·10⁻⁶ for 10⁻¹¹ M MeHg, log₂FC 3.55 and FDR 1.50·10⁻¹³ for 10⁻¹⁰ M MeHg, log₂FC 3.66 and FDR 1.30·10⁻¹⁴ for 10⁻⁹ M MeHg, 4.37 and FDR 1.50·10⁻²³ for 10⁻⁸ M MeHg). In addition, IHg and MeHg exposure also influenced genes involved in the tricarboxylic acid (TCA) cycle. This metabolism occurs in the mitochondria, supporting evidence that both Hg forms affected mitochondrial activity and therefore the whole energy metabolism.

At the physiological level, chlorophyll *a* content ([chl *a*]) was increased at 10⁻¹⁰ M IHg vs control while photosynthesis efficiency was increased for 10⁻¹¹ and 10⁻¹⁰ M IHg and in all MeHg exposure concentrations vs control (Table 2). This increase followed a “bell shape” with a higher increase for intermediate concentrations of exposure, typical of a hormesis effect, resulting from overcompensating for a moderate stress²⁸. Along the same lines, a recent study reported a hormetic effect on photosynthesis efficiency in *C. reinhardtii* at 10⁻¹¹ and 10⁻¹⁰ M MeHg¹². Interestingly, it was found that phototrophic bacteria growth rates increased with increasing IHg concentrations suggesting that Hg could fulfil a physiological function²⁹. However here, at higher [THg]_{water} [chl *a*] tended to decrease (Table 2) in line with expected toxicity pathways of Hg^{6,7}. Nevertheless, transcriptomics and physiological analysis revealed here that *C. reinhardtii* was able to cope with the tested Hg concentrations and developed an efficient tolerance response.

Reduction–oxidation reaction (RedOx) homeostasis. IHg and MeHg impacted the expression of genes involved in RedOx homeostasis such as thioredoxin (both up- and down- regulated by IHg and MeHg), peroxiredoxin (4 and 2 genes up-regulated at 10⁻⁸ M MeHg and IHg, respectively), and cytochrome p450 (1 to 6 and 11 to 15 up-regulated genes in the case of IHg and MeHg, respectively). Glutathione peroxidase were also up-regulated at 10⁻⁸ M MeHg (Cre03.g197750.t1.2, GPX3, log₂FC 1.41, and FDR 1.54·10⁻⁷), and 10⁻⁸ M IHg concentration (Cre10.g458450, GPX5, log₂FC 1.05, and FDR 3, 15·10⁻⁴). These observations point to an enhancement of reactive oxygen species (ROS) production induced by MeHg and IHg, in accordance with expected toxicity, and a subsequent modification of the RedOx homeostasis network in *C. reinhardtii*^{6,7}. For example, thioredoxin are key molecules in the response of plants to oxidative stress induced by toxic metals^{30–32}. On the other hand, at the physiological level, a significant increase of the intracellular ROS was only observed at 10⁻¹⁰ M MeHg but there was no impact for all IHg and MeHg treatments on membrane permeability, which can result from ROS-dependent lipid peroxidation (Table 2). Oxidative stress occurs from imbalance in RedOx homeostasis in cells which results in an overproduction of ROS. Strong ROS production is expected for soft Lewis acids such as Hg²⁺ and CH₃Hg⁺ and when photosynthesis and mitochondria are impacted as suggested by the genes dysregulated here (see the subsection *Energy metabolism* above). Here, RedOx homeostasis seems to be more strongly influenced by MeHg than IHg at the gene level, similar to all the other categories. However, the algal cells limit ROS enhancement through an efficient antioxidant response observed at the gene level, which results in an absence of oxidative stress (except at 10⁻¹⁰ M MeHg) and agrees with observations previously reported for MeHg in *C. reinhardtii*¹².

Amino acid, lipid, and other metabolisms. IHg and MeHg exposure resulted in the dysregulation of genes involved in the metabolism of the thiol-related amino acids - glutamate, cysteine, and methionine- as well as biotin (acetyl-coenzyme A [CoA] cofactor) (Table 1, Tables S3 and S4). Biotin -a cofactor of acetyl CoA involved in sulfur (S) metabolism- was significantly enriched in response to MeHg (e.g. Cre17.g733650.t1.3, biotin F, log₂FC 0.95 and FDR 3.53·10⁻⁴, log₂FC 1.02 and FDR 8.64·10⁻⁵, log₂FC 1.01 and FDR 1.03·10⁻⁴, for 10⁻¹¹, 10⁻¹⁰ and 10⁻⁹ M MeHg, respectively). Increased biosynthesis of biotin was observed in *C. reinhardtii* under conditions of S-deprivation³³. The data presented here supports dysregulation of S metabolism in the presence of MeHg. S could be useful for detoxifying sequestration of IHg and MeHg as thiol groups have high affinity to Hg. For example,

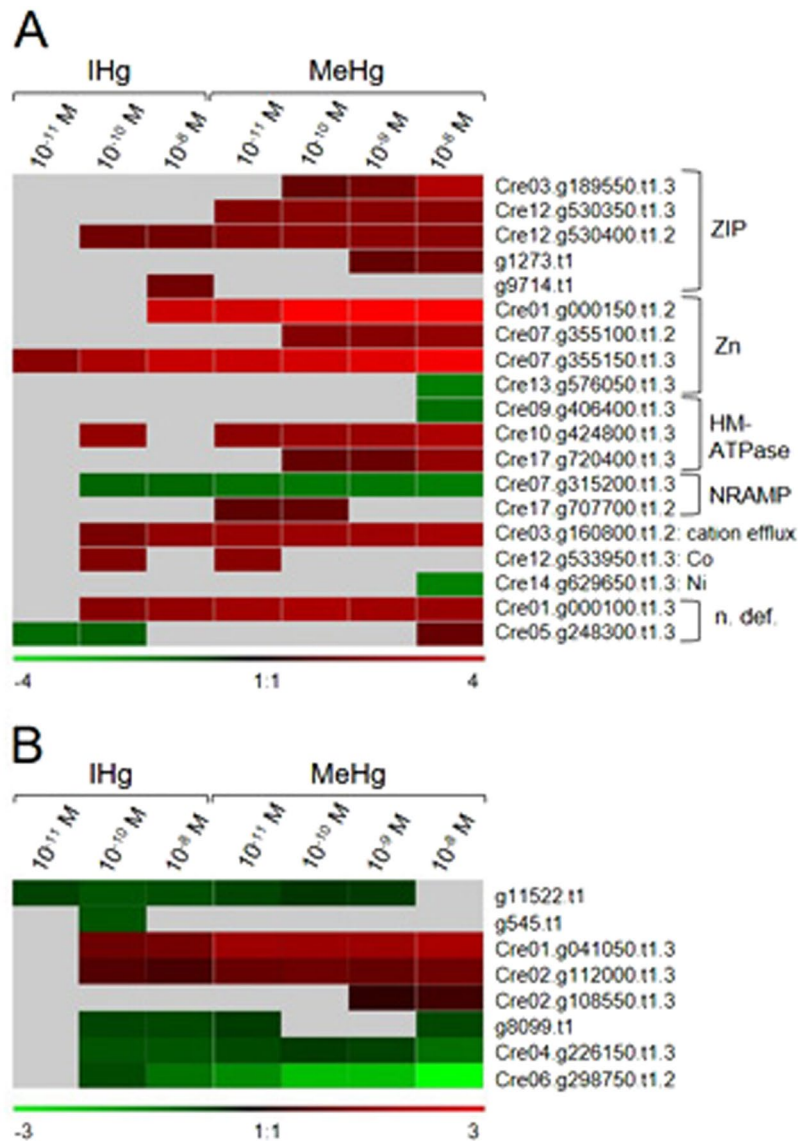


Figure 3. Gene expression regulation of 19 metal (A) and 8 amino acid (B) transporters significantly dysregulated in *C. reinhardtii* exposed 2 h to IHg or MeHg (ZIP = zinc-, iron-regulated transporter family; Zn = zinc transporter precursors; HM-ATPase = heavy metal ATPase; NRAMP = natural resistance-associated macrophage protein metal ion transporter family protein; Co = cobalt ion transmembrane transporter; Ni = high-affinity nickel-transport family protein; n. def. = no definition) (Phytozome V9.0).

S-containing amino acids (i.e. methionine and cysteine) and the subsequently biosynthesized S-rich peptides, phytochelatins (PC) and glutathione (GSH) can act as chelating molecules^{34,35} and could here be involved in a mechanism of tolerance to MeHg in *C. reinhardtii*.

Transport. Since the effects of contaminants depend on the intracellular concentration and their fate, the understanding of the uptake pathways and corresponding gene expression levels are of the highest interest. Genes involved in transporting metabolites, adenosine triphosphate (ATP) Binding Cassette (ABC) transporters, and metal transporters were dysregulated in all Hg treatments and similarly as in other categories, the number of dysregulated genes increased with $[\text{THg}]_{\text{intra}}$ and was higher for MeHg than IHg (Table 1, Fig. 3). It is therefore tempting to hypothesize that several of these transporters are involved in Hg tolerance/detoxification mechanisms. Among the dysregulated ABC transporters, the multidrug resistance-associated protein 2 (MRP2), which was dysregulated in response to both Hg species here, has been identified as central in the transport of metals (e.g. cadmium; Cd) to the vacuole for detoxification³⁶. Similarly, here these transporters could be involved in Hg vacuole detoxification, a well-known tolerance mechanism for toxic metals in primary producers³⁴. Furthermore, genes involved in calcium (Ca^{2+}) and S transport were significantly dysregulated by both IHg and MeHg. These regulations suggest an increase of intracellular ROS production. Indeed, Ca^{2+} has a major function as intracellular messenger, and act in concert with ROS signaling pathways in various cell processes such as growth and

phototaxis in *C. reinhardtii*^{37,38}. Significantly, an increase of ROS production causes an increase of $[Ca^{2+}]_{intra}$ and vice-versa³⁹. Similarly, S transport is linked to the thiol pool that can play a role in Hg chelation and vacuolar compartmentation as well as in ROS scavenging by stimulating increases in glutathione biosynthesis⁴⁰. This hypothesis agrees with the induction of genes involved in RedOx homeostasis by IHg and MeHg exposure in *C. reinhardtii* discussed in the section concerning *RedOx homeostasis* (see above).

Several zinc (Zn)-regulated transporters iron (Fe)-regulated transporter-like Proteins (ZIP) transporters of Fe and Zn as well as Zn transporters were also up-regulated by IHg and MeHg (Fig. 3A,B). At the higher concentration of MeHg, the nickel (Ni) high-affinity transporter, a heavy metal ATPase, and a Zn transporter were down-regulated. These observations suggest impact of IHg and MeHg on the global nutrition of the microalgae, and are in line with what has been observed in bacteria and plants in which essential-metal transporters are considered as potential uptake pathways for Hg^{21,41}. Indeed, a competition between IHg and Cu uptake was observed in *Eloдея nuttallii* as well as IHg and Zn uptake in bacteria^{21,41,42}. In addition, a close chemical mimicry exists between cysteine-MeHg and methionine, the hypothesis being made that the mechanism of Hg uptake in bacteria could be through amino-acid transporters^{43–45}. Overall, here both IHg and MeHg dysregulated transporters are involved in nutrition, metal homeostasis, and in amino acid transport, suggesting that Hg may enter cells and/or be detoxified by those transporters. Further studies, notably identification and functional characterization of specific transporters, are needed to unambiguously demonstrate the carrier-mediated transport of Hg.

Genes specific to IHg and MeHg exposures. Overall comparison of genes dysregulated by IHg and MeHg exposures showed an absence of specific expression response to IHg (Table S5). Nonetheless, further detailed analysis of the genes specifically dysregulated for a given concentration, revealed differences in the proportion of the genes responding specifically to IHg treatments in some of the metabolic pathways. For example, 33% and 67% of genes specifically down-regulated at 10^{-11} M IHg were involved in development and stress, whilst these percentages were only 9% and 8% at 10^{-11} M MeHg exposure (Table S5). Genes involved in secondary metabolism represented 12% or 2% of specifically up-regulated genes by 10^{-11} M IHg or MeHg respectively (Table S5). Similarly, bigger percentage (11% up and 20% down) of genes involved in the stress category specific at 10^{-10} M IHg treatment were found in comparison with the same exposure concentration for MeHg (2% up and 8% down) (Table S5). Analogical trends were found for genes involved in lipid metabolism and mitochondrial electron transport/ATP synthesis specifically down-regulated by 10^{-8} M IHg and MeHg. Other metabolic pathways were more represented in MeHg treatments, probably due to the bias of the higher number of genes responding to MeHg, resulting in very limited IHg-specific impacted biological pathways. To reduce this bias, we thus compared IHg and MeHg treatments showing a closer number of dysregulated genes, namely the highest IHg concentration (2836 genes) and the lowest MeHg concentration (4174 genes; Table S6). As before, none of the metabolic pathways was dysregulated specifically by IHg and genes dysregulated by MeHg were found in more categories than those dysregulated by IHg (29 and 17, respectively). Genes involved in energy metabolism and development appeared to represent a higher proportion of genes specifically dysregulated by 10^{-8} M IHg than by 10^{-11} M MeHg, while genes involved in lipid metabolism represent a higher proportion of genes specifically dysregulated by 10^{-11} M MeHg than by 10^{-8} M IHg.

Considering the complete set of significantly dysregulated genes by IHg or MeHg, 134 genes were found to be specifically dysregulated by IHg treatments; however 96 of these genes have an unidentified function (Table 3). Similarly from the 5493 genes specifically dysregulated by MeHg, 3569 had an unidentified function. Globally IHg dysregulated genes were attributed to 16 categories, while MeHg dysregulated genes were attributed to 34 categories and none of the metabolic pathway was specific to IHg. Further analysis revealed that only 19 common genes were significantly dysregulated specifically by the three IHg treatments, while 981 genes were unique to the four MeHg treatments and absent in responses to IHg (Table 3). These findings show a stronger and more specific response of *C. reinhardtii* to MeHg exposure. However, 63% of genes specifically responding to MeHg exposure have an unknown function, 19% are related to gene expression regulation and signaling, 4% to cell organization and motility, 4% to transport, 1% to amino acids metabolism, and 1% to lipid metabolism. Similarly, for IHg, 10 of 19 genes have an unknown function, the others being involved in gene regulation and signaling, transport, cell processes, and development.

Therefore, specific genes responding to MeHg includes notably a higher proportion of transporters, nevertheless no clear conclusions can be drawn about possible difference between MeHg and IHg subcellular targets and tolerance responses in *C. reinhardtii* in terms of dysregulated categories of genes as similar responses are observed and specific responses include many unknown genes.

Conclusion

This study highlighted the molecular-level responses of green microalga *C. reinhardtii*, a representative primary producer, to a broad range of environmental exposure concentrations of IHg or MeHg (Fig. 4). For similar $[THg]_{water}$ exposure to MeHg resulted in a higher $[THg]_{intra}$ in *C. reinhardtii* compared with exposure to IHg. The number of dysregulated genes increased with the intracellular concentrations for both IHg and MeHg exposure. However, for comparable intracellular concentrations $[THg]_{intra}$, MeHg exposure dysregulated a larger number of genes than IHg exposure, supporting different subcellular fate of IHg and MeHg at similar concentrations in *C. reinhardtii*. Nevertheless, IHg and MeHg dysregulated similar categories of genes involved in cell processes, energy metabolism, photosystems, and RedOx homeostasis in agreement with expected toxicity. In addition, genes involved in cell motility, nutrition, and amino acids metabolism were dysregulated including during exposure to low environmental concentrations, revealing a broader impact on *C. reinhardtii* metabolism than expected based on physiological endpoints. Despite the strong gene response for both IHg and MeHg, the respective physiological responses were low. Only one treatment resulted in a significant increase of the cellular ROS and oxidative stress (10^{-10} M MeHg, Table 2), suggesting that the microalga could cope with the range of concentrations of

| Metabolic pathways | Number of genes | | | |
|--|---------------------|------|----------|------|
| | Specific and common | | Specific | |
| | IHg | MeHg | IHg | MeHg |
| Amino acid metabolism | | 12 | 1 | 66 |
| Biodegradation of Xenobiotics | | 1 | | 8 |
| C1-metabolism | | 2 | | 7 |
| Cell processes | 1 | 41 | 2 | 147 |
| Cell wall | | | | 10 |
| Co-factor and vitamine metabolism | | 4 | | 22 |
| Development | 1 | 8 | 1 | 38 |
| DNA | | 24 | 1 | 113 |
| Fermentation | | | | 2 |
| Gluconeogenesis/glyoxylate cycle | | 1 | | 4 |
| Glycolysis | | 3 | | 14 |
| Hormone metabolism | | 2 | 1 | 16 |
| Lipid metabolism | | 11 | 1 | 74 |
| Major CHO metabolism | | 5 | | 22 |
| Minor CHO metabolism | | 4 | | 20 |
| Metal handling | | | | 7 |
| Miscellaneous | | 20 | 4 | 101 |
| Mitochondrial electron transport/ ATP synthesis | | 2 | | 10 |
| N-metabolism | | 1 | | 14 |
| Nucleotide metabolism | | 7 | | 32 |
| OPP | | | | 3 |
| Polyamine metabolism | | | | 3 |
| Photosynthesis | | 1 | 3 | 54 |
| Protein | 4 | 116 | 5 | 536 |
| Redox | | 3 | 1 | 31 |
| RNA | 2 | 54 | 6 | 238 |
| S-assimilation | | | | 3 |
| Secondary metabolism | | 1 | 1 | 25 |
| Signaling | 1 | 14 | 2 | 66 |
| Stress | | 7 | | 30 |
| TCA/org transformation | | 2 | | 11 |
| Tetrapyrrole synthesis | | 4 | 3 | 16 |
| Transport | 1 | 38 | 6 | 161 |
| Unknown | 10 | 606 | 96 | 3569 |
| Total | 20 | 994 | 134 | 5493 |

Table 3. Number of significantly dysregulated genes in metabolic pathways (MapMan) specifically responding to IHg or MeHg (specific) and common to all tested concentrations (specific and common) in *C. reinhardtii* after 2 h exposure.

IHg and MeHg tested here (10^{-11} to 10^{-8} M), at least for a short-exposure period. Overall, a detailed mechanistic understanding of differences in cellular handling of IHg and MeHg resulting in a stronger impact of MeHg were obtained from the analysis of the uptake and perturbations of the cell's functions presented in this paper (Fig. 4). This knowledge is central for the development of integrated effect assessments and predicting the impact of toxicants on organisms.

Methods

Algal culture and exposure conditions. The unicellular green alga *Chlamydomonas reinhardtii* (wild type strain CPCC11) was obtained from the Canadian Phycological Culture Centre (CPCC, Department of Biology, University of Waterloo, Waterloo, ON, Canada). Cultures were grown in a specialized incubator (Multitron Infors HT, Bottmingen, Switzerland) at 20.2 ± 0.5 °C with a 24-h light cycle (3600 lux) and a constant 115 rpm rotary shaking. Cells were grown in a 4× diluted Tris-Acetate-Phosphate medium (Harris, 1989) containing tris-acetate, ammonium, phosphate, ethylenediaminetetraacetic acid (EDTA) and metals (B, Mn, Fe, Zn, Co, Mo, Cu) at pH 7.0.

For the exposures, cells were harvested in their middle exponential growth phase (62 h post inoculation) by centrifugation (10 min at 1300 g) and washed once with Hg free exposure medium ($8.2 \cdot 10^{-4}$ M CaCl₂, $3.6 \cdot 10^{-4}$ M MgSO₄, $2.8 \cdot 10^{-4}$ M NaHCO₃, $1.0 \cdot 10^{-4}$ M KH₂PO₄ and $5.0 \cdot 10^{-6}$ M NH₄NO₃ at pH 6.9 ± 0.1). Subsequently cells were centrifuged again and re-suspended in the exposure medium. Cells were then exposed in the same incubator

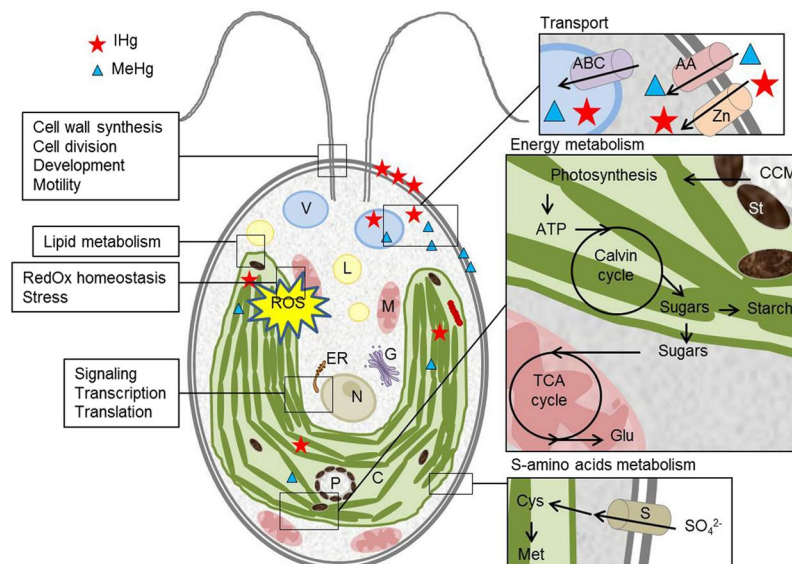


Figure 4. Schematic representation of cellular toxicity pathways and tolerance responses, as derived from uptake, transcriptome and physiological effects in *C. reinhardtii* exposed 2 h to IHg and MeHg (AA: amino acid transporter; ABC: ABC transporter; C: chloroplast; CCM: carbon concentrating mechanism; Cys: cysteine; L: lipid bodies; ER: endoplasmic reticulum; G: golgi; Glu: glutamate; M: mitochondria; Met: methionine; N: nucleus; P: pyrenoid; S: S transporter; St: starch; V: vacuole; Zn: metal transporter).

(see conditions above) at a cell density of $1 \cdot 10^6$ cells \cdot mL $^{-1}$ for 2 h. This exposure duration was chosen based on toxicokinetics results for *C. reinhardtii* to both identify early response genes at the transcriptome level and reach measurable bioaccumulation¹².

All materials were washed in 10% HNO₃ followed by 10% HCl acid baths, thoroughly rinsed with ultrapure water (MilliQ Direct system, Merck Millipore, Darmstadt, Germany) and dried under a laminar flow hood. Material for culture and experiments, including media, were additionally autoclaved (1 bar, 121 °C, 20 min) to avoid microbial contamination.

Hg bioaccumulation in *C. reinhardtii* and speciation. *C. reinhardtii* cells were exposed to 10^{-11} , 10^{-10} or 10^{-8} M IHg using Hg(NO₃) standard solution (Sigma-Aldrich, Buchs, Switzerland) or 10^{-11} , 10^{-10} , 10^{-9} or 10^{-8} M MeHg using MeHgCl standard solution (Alfa Aesar, Ward Hill, MA, USA). Cells exposed in the absence of Hg in the exposure medium were used as control. Exposure medium samples were preserved in the dark at 4 °C with 0.5% Suprapur® HCl (Merck, Darmstadt, Germany).

Speciation of IHg and MeHg in the exposure medium was computed using the Windermere Humic Aqueous Model (WHAM) model VII⁴⁶. Its default database was updated for OH⁻, Cl⁻, SO₄²⁻ and CO₃²⁻ binding constants⁴⁷.

At the end of the exposure, two aliquots ($\times 3$ replicates) of 50 mL were sub-sampled. After centrifugation, cells in the pellet were washed once with Hg-free exposure medium. The pellet of one of the aliquots was kept to measure the “whole cell” Hg concentration ([THg]_{intra+ads}). The second aliquots were re-suspended in 10^{-3} M EDTA for IHg or 10^{-3} M EDTA + 10^{-3} M cysteine (Sigma-Aldrich, Buchs, Switzerland) for MeHg prepared in the exposure medium, to rinse adsorbed or loosely bound to the cell wall Hg to determine the intracellular Hg concentrations ([THg]_{intra})⁴⁸. All pellets were freeze-dried (Beta 1–8 K, Christ, Germany) and kept in the dark until analysis.

Total Hg (THg = IHg + MeHg) concentration in algae was determined by atomic absorption spectrometry using the Advanced Hg Analyzer AMA 254 (Altec s.r.l., Czech Republic). Detection limit defined as $3 \times$ the standard deviation (s.d.) of 10 blank measurements was 0.05 ng_{THg}. The accuracy of the measurements was checked by analyzing the certified reference material (CRM) MESS-3 ($100 \pm 0.1\%$ recovery). Exposure medium samples were analyzed for initial THg concentrations with the MERX® Automated Total Mercury Analytical System (Brooks Rand Instruments, Seattle, WA, USA). Detection limit was 0.03 ng_{THg} \cdot L $^{-1}$. The accuracy of THg measurements was tested by analyzing the CRM ORMS-5 ($116.0 \pm 3.5\%$ recovery). MeHg concentration was measured in exposure medium samples and in algae after mineralization 12 h at 60 °C with 30% HNO₃ suprapur® (Merck, Darmstadt, Germany) with the instrument MERX® Automated Methylmercury Analytical System (Brooks Rand Instruments, Seattle, WA, USA) following the United State of America Environmental Protection Agency (US EPA) Method 1630⁴⁹ and manufacturer instructions. Detection limit was 0.01 ng_{MeHg} \cdot L $^{-1}$. The accuracy of MeHg measurements was tested by analyzing the CRM TORT-2. Its recovery was $57.1 \pm 5.3\%$.

RNA-Seq and differential gene expression analysis. *Total RNA extraction.* At the end of the exposure, $\sim 10^7$ cells were harvested by centrifugation (10 min at 1300 g) in triplicates and immediately frozen in liquid nitrogen and stored 1 night at -80 °C before total RNA extraction was conducted. For this, 0.5 mL of steel beads (0.50–0.75 mm, Retsch, Haan, Germany) and 1 mL TRI Reagent® (Sigma-Aldrich, Buchs, Switzerland) were added to the frozen algal pellet and the samples were shaken 30 s at 30 Hz (Mixer Mill MM 400, Retsch

GmbH, Haan, Germany). Total RNA was then extracted following provider's instructions. The amount and quality of RNA was confirmed by electrophoresis gel, measurement of total RNA concentration with Qubit® (Life Technologies Europe, Zug, Switzerland) and Agilent Bioanalyzer RNA 6000 Nano Kit (Agilent Technologies Inc., Santa Clara, CA, USA).

Library preparation and sequencing. Libraries were prepared following manufacturer's protocols (Illumina, San Diego, CA, USA) and sequenced on an Illumina HiSeq. 2500 System (Illumina, San Diego, CA, USA), generating single-end reads of 100 bp. Data quality was controlled using the open source software FastQC (www.bioinformatics.babraham.ac.uk/projects/fastqc/).

Bioinformatics pipeline and differential gene expression analysis. Samples were aligned with TopHat2 to the *Creinhardtii* 236 V.9.0 available at phytozome.org, and genes sequences and annotations were retrieved (<ftp://ftp.jgi-psf.org/pub/compugen/phytozome/v9.0/Creinhardtii/annotation/>). Reads were counted using the Python package HTSeq⁵⁰. Data were deposited in the Gene Expression Omnibus database (GSE65109).

Differential gene expression analysis. Comparison of each IHg and MeHg conditions vs. Control generated fold change (FC) and false discovery rate adjusted *p*-values (FDR) was performed in the software CLC Main Workbench (Version 7, CLC bio, QIAGEN, Denmark) based on normalized counts and EdgeR package⁵¹. Significant differently expressed transcripts vs. control were defined with a threshold of false discovery rate (FDR) < 0.1% and of fold change log₂ transformed (log₂FC). Venn diagrams were realized with <http://bioinformatics.psb.ugent.be/webtools/Venn/>.

Functional annotation and enrichment analyses. Ontology term assignments were done using MapMan (Version 3.6.0RC1)^{52, 53}. Wilcoxon test were used to identify most strongly dysregulated categories in each treatment (*p* < 0.05). Gene information was also retrieved using AlgaePath and the Algal Functional Annotation Tool^{54, 55}.

Reverse transcriptase quantitative Polymerase Chain Reaction (RT-qPCR). To validate the RNAseq, RT-qPCR analysis was performed. Details can be found in the Supporting information.

Physiological endpoints. The effects of IHg and MeHg on algal physiology were assessed by studying four endpoints for all the tested concentrations. The *oxidative stress* level of cells was assessed by the presence of intracellular ROS with the fluorescent probe Cell Rox Green Reagent® (Life Technologies Europe, Zug, Switzerland) added to a 1 mL subsample at a final concentration of 5·10⁻⁶ M. After 30 min incubation in the dark, the percentage of cells suffering from oxidative stress was assessed by flow cytometry (BD Accuri C6, BD Biosciences, Allschwil, Switzerland) with the detector FL1 (530 ± 15 nm) (positive control: cells exposed 1 h to 2·10⁻⁴ M 30% H₂O₂ (Suprapur®, Merck Millipore, Darmstadt, Germany)). To assess the viability of the cells, *membrane integrity* was measured with propidium iodide (Sigma-Aldrich, Buchs, Switzerland), a fluorescent intercalating agent, added to the sample at a final concentration of 7·10⁻⁶ M and analyzed with the detector FL2 (585 ± 20 nm) of the flow cytometer (positive control: cells exposed 30 min to 1·10⁻² M H₂O₂). The *efficiency of the photosynthesis* was assessed using Fast repetition rate fluorometry (FRRf) on 30 min dark adapted algae^{56, 57}. The ratio of variable fluorescence (F_v) over maximum fluorescence (F_m) was measured indicating the maximum potential efficiency of photosystem II. The *chlorophyll a content* ([chl *a*]) was additionally determined with the Trilogy® Laboratory Fluorometer equipped with the chlorophyll *a in vivo* module (Turner Designs, Sunnyvale, CA, USA.).

Data analyses. Data were tested for normality (Shapiro-Wilk, $\alpha = 0.01$) and homoscedasticity ($\alpha = 0.01$) and subsequently Student t-test was applied to compare treated vs. control samples. All statistical analyses and plots were computed using Sigma Plot® V12.5 (Systat Software, Inc., San Jose, CA, USA). Clusters and heatmaps were computed with Genesis v1.7.7 (Institute for Genomics and Bioinformatics, Graz University of Technology, Graz, Austria)⁵⁸.

References

1. Sunderland, E. M. & Schartup, A. T. Biogeochemistry: Mercury methylation on ice. *Nat Microbiol* **1**, 16165 (2016).
2. Yin, R. *et al.* Historical records of mercury stable isotopes in sediments of Tibetan lakes. *Sci Rep* **6**, 23332 (2016).
3. Poulain, A. J. *et al.* Microbial DNA records historical delivery of anthropogenic mercury. *ISME J* **9**(12), 2541–2550 (2015).
4. Armstrong, A. Mercury and plants. *Nature Geosci* **5**(3), 160–160 (2012).
5. Lehnher, I. St. Louis, V. L., Hintelmann, H. & Kirk, J. L. Methylation of inorganic mercury in polar marine waters. *Nature Geosci* **4**(5), 298–302 (2011).
6. Cosio, C., Flück, R., Regier, N. & Slaveykova, V. I. Effects of macrophytes on the fate of mercury in aquatic systems. *Environ Toxicol Chem* **33**(6), 1225–1237 (2014).
7. Le Faucheur, S., Campbell, P. G. C., Fortin, C. & Slaveykova, V. I. Interactions between mercury and phytoplankton: Speciation, bioavailability, and internal handling. *Environ Toxicol Chem* **33**(6), 1211–1224 (2014).
8. Dranguet, P. *et al.* Towards mechanistic understanding of mercury availability and toxicity to aquatic primary producers. *CHIMIA Int J Chem* **68**(11), 799–805 (2014).
9. Bravo, A. G. *et al.* Extremely elevated methyl mercury levels in water, sediment and organisms in a Romanian reservoir affected by release of mercury from a chlor-alkali plant. *Water Res* **49**, 391–405 (2014).
10. Wu, Y., Zeng, Y., Qu, J. Y. & Wang, W.-X. Mercury effects on *Thalassiosira weissflogii*: Applications of two-photon excitation chlorophyll fluorescence lifetime imaging and flow cytometry. *Aqu Toxicol* **110–111**, 133–140 (2012).
11. Boening, D. W. Ecological effects, transport, and fate of mercury: a general review. *Chemosphere* **40**(12), 1335–1351 (2000).

12. Beauvais-Fluck, R., Slaveykova, V. I. & Cosio, C. Transcriptomic and physiological responses of the green microalga *Chlamydomonas reinhardtii* during short-term exposure to subnanomolar methylmercury concentrations. *Environ Sci Technol* **50**(13), 7126–7134 (2016).
13. Watanabe, H. & Iguchi, T. Using ecotoxicogenomics to evaluate the impact of chemicals on aquatic organisms. *Marine Biol* **149**(1), 107–115 (2006).
14. Pillai, S. *et al.* Linking toxicity and adaptive responses across the transcriptome, proteome, and phenotype of *Chlamydomonas reinhardtii* exposed to silver. *Proc Natl Acad Sci U S A* **111**(9), 3490–3495 (2014).
15. EU, DIRECTIVE 2013/39/EU OF THE EUROPEAN PARLIAMENT AND OF THE COUNCIL of 12 August 2013 amending Directives 2000/60/EC and 2008/105/EC as regards priority substances in the field of water policy. *Official Journal of the European Union* L226 (2013).
16. Guigues, S., Bravin, M. N., Garnier, C. & Doelsch, E. Does specific parameterization of WHAM improve the prediction of copper competitive binding and toxicity on plant roots? *Chemosphere* **170**, 225–232 (2017).
17. Bravo, A. G., Le Faucheur, S., Monperrus, M., Amouroux, D. & Slaveykova, V. I. Species-specific isotope tracers to study the accumulation and biotransformation of mixtures of inorganic and methyl mercury by the microalga *Chlamydomonas reinhardtii*. *Environ Poll* **192**(0), 212–215 (2014).
18. Ndu, U., Mason, R. P., Zhang, H., Lin, S. & Visscher, P. T. Effect of inorganic and organic ligands on the bioavailability of methylmercury as determined by using a mer-lux bioreporter. *Appl Environ Microbiol* **78**(20), 7276–7282 (2012).
19. Moyer, H. A., Miles, C. J., Philips, E. J., Sargent, B. & Merritt, K. K. Kinetics and uptake mechanisms for monomethylmercury between freshwater algae and water. *Environ Sci Technol* **36**(16), 3550–3555 (2002).
20. Pickhardt, P. C. & Fisher, N. S. Accumulation of inorganic and methylmercury by freshwater phytoplankton in two contrasting water bodies. *Environ Sci Technol* **41**(1), 125–131 (2007).
21. Regier, N. *et al.* Mercury bioaccumulation in the aquatic plant *Elodea nuttallii* in the field and in microcosm: Accumulation in shoots from the water might involve copper transporters. *Chemosphere* **90**(2), 595–602 (2013).
22. Wang, W. X., Wong, R. S., Wang, J. & Yen, Y. F. Influences of different selenium species on the uptake and assimilation of Hg(II) and methylmercury by diatoms and green mussels. *Aquat Toxicol* **68**(1), 39–50 (2004).
23. Liu, G. *et al.* Toxicity of copper, lead, and cadmium on the motility of two marine microalgae *Isochrysis galbana* and *Tetraselmis chui*. *J Environ Sci* **23**(2), 330–335 (2011).
24. Khona, D. K. *et al.* Characterization of salt stress-induced palmelloids in the green alga. *Chlamydomonas reinhardtii*. *Algal Res* **16**, 434–448 (2016).
25. Grennan, A. K. Plastoglobule proteome. *Plant Physiol* **147**(2), 443–445 (2008).
26. Xiang, Y. B., Zhang, J. & Weeks, D. P. The *Cia5* gene controls formation of the carbon concentrating mechanism in *Chlamydomonas reinhardtii*. *Proc Natl Acad Sci USA* **98**(9), 5341–5346 (2001).
27. Duanmu, D., Miller, A. R., Horken, K. M., Weeks, D. P. & Spalding, M. H. Knockdown of limiting-CO₂-induced gene *HLA3* decreases HCO₃⁻ transport and photosynthetic Ci affinity in *Chlamydomonas reinhardtii*. *Proc Natl Acad Sci USA* **106**(14), 5990–5995 (2009).
28. Poschenrieder, C., Cabot, C., Martos, S., Gallego, B. & Barcelo, J. Do toxic ions induce hormesis in plants? *Plant Sci* **212**, 15–25 (2013).
29. Gregoire, D. S. & Poulain, A. J. A physiological role for Hg^{II} during phototrophic growth. *Nature Geosci* **9**(2), 121–125 (2016).
30. Lemaire, S. D. *et al.* New thioredoxin targets in the unicellular photosynthetic eukaryote *Chlamydomonas reinhardtii*. *Proc Natl Acad Sci USA* **101**(19), 7475–7480 (2004).
31. Gillet, S., Decottignies, P., Chardonnet, S. & Le Marechal, P. Cadmium response and redoxin targets in *Chlamydomonas reinhardtii*: a proteomic approach. *Photosynth Res* **89**(2–3), 201–211 (2006).
32. Montrichard, F. *et al.* Thioredoxin targets in plants: The first 30 years. *J Proteomics* **72**(3), 452–474 (2009).
33. Gonzalez-Ballester, D. *et al.* RNA-seq analysis of sulfur-deprived *Chlamydomonas* cells reveals aspects of acclimation critical for cell survival. *Plant Cell* **22**(6), 2058–2084 (2010).
34. Park, J. *et al.* The phytochelatin transporters AtABCC1 and AtABCC2 mediate tolerance to cadmium and mercury. *Plant J: Cell Molec Biol* **69**(2), 278–288 (2012).
35. Wu, Y. *et al.* Quantitative relationship between cadmium uptake and the kinetics of phytochelatin induction by cadmium in a marine diatom. *Sci Rep* **6**, 35935 (2016).
36. Simon, D. F., Descombes, P., Zerges, W. & Wilkinson, K. J. Global expression profiling of *Chlamydomonas reinhardtii* exposed to trace levels of free cadmium. *Environ Toxicol Chem* **27**(8), 1668–1675 (2008).
37. Kudla, J., Batistio, O. & Hashimoto, K. Calcium signals: the lead currency of plant information processing. *Plant Cell* **22**(3), 541–563 (2010).
38. Wakabayashi, K.-i., Misawa, Y., Mochiji, S. & Kamiya, R. Reduction-oxidation poise regulates the sign of phototaxis in *Chlamydomonas reinhardtii*. *Proc Natl Acad Sci* **108**(27), 11280–11284 (2011).
39. Steinhilber, L. & Kudla, J. Calcium and reactive oxygen species rule the waves of signaling. *Plant Physiol* **163**(2), 471–485 (2013).
40. Gomes, M. P., Soares, A. M. & Garcia, Q. S. Phosphorous and sulfur nutrition modulate antioxidant defenses in *Myracrodruon urundeuva* plants exposed to arsenic. *J Haz Mat* **276**, 97–104 (2014).
41. Szczuka, A., Morel, F. M. M. & Schaefer, J. K. Effect of thiols, zinc, and redox conditions on Hg uptake in *Shewanella oneidensis*. *Environ Sci Technol* **49**(12), 7432–7438 (2015).
42. Schaefer, J. K., Szczuka, A. & Morel, F. M. M. Effect of divalent metals on Hg(II) uptake and methylation by bacteria. *Environ Sci Technol* **48**(5), 3007–3013 (2014).
43. Schaefer, J. K. & Morel, F. M. M. High methylation rates of mercury bound to cysteine by *Geobacter sulfurreducens*. *Nature Geosci* **2**(2), 123–126 (2009).
44. Schaefer, J. K. *et al.* Active transport, substrate specificity, and methylation of Hg(II) in anaerobic bacteria. *Proc Natl Acad Sci USA* **108**(21), 8714–8719 (2011).
45. Bridges, C. C. & Zalups, R. K. Transport of inorganic and methylmercury in target tissues and organs. *J Toxicol Environ Health-Part B-Crit Rev* **13**(5), 385–410 (2010).
46. Tipping, E., Lofts, S. & Sonke, J. E. Humic ion-binding model VII: a revised parameterisation of cation-binding by humic substances. *Environ Chem* **8**(3), 225–235 (2011).
47. Powell Kipton, J. *et al.* Chemical speciation of environmentally significant heavy metals with inorganic ligands. Part 1: The Hg²⁺-Cl⁻, OH⁻, CO₃²⁻, SO₄²⁻, and PO₄³⁻-aqueous systems (IUPAC Technical Report). *pac* doi:10.1351/pac200577040739 (2005).
48. Larras, F. *et al.* Physiological and proteomic changes suggest an important role of cell walls in the high tolerance to metals of *Elodea nuttallii*. *J Haz Mat* **263**(2), 575–583 (2013).
49. USEPA, Method 1630: Methyl mercury in water by distillation, aqueous ethylation, purge and trap, and CVAFS. USEPA, Office of Water (2001).
50. Anders, S., Pyl, P. T. & Huber, W. HTSeq—a Python framework to work with high-throughput sequencing data. *Bioinformatics* **31**(2), 166–169 (2014).
51. Robinson, M. D., McCarthy, D. J. & Smyth, G. K. edgeR: a Bioconductor package for differential expression analysis of digital gene expression data. *Bioinformatics* **26**(1), 139–140 (2010).

52. Usadel, B. *et al.* A guide to using MapMan to visualize and compare Omics data in plants: a case study in the crop species, Maize. *Plant Cell Environ* **32**(9), 1211–1229 (2009).
53. Thimm, O. *et al.* MAPMAN: a user-driven tool to display genomics data sets onto diagrams of metabolic pathways and other biological processes. *Plant j: cell molec biol* **37**(6), 914–939 (2004).
54. Zheng, H. Q. *et al.* AlgaePath: comprehensive analysis of metabolic pathways using transcript abundance data from next-generation sequencing in green algae. *BMC Genomics* **15**, 196 (2014).
55. Lopez, D., Casero, D., Cokus, S., Merchant, S. & Pellegrini, M. Algal functional annotation tool: a web-based analysis suite to functionally interpret large gene lists using integrated annotation and expression data. *BMC Bioinformatics* **12**(1), 282 (2011).
56. Kolber, Z. S., Prasil, O. & Falkowski, P. G. Measurements of variable chlorophyll fluorescence using fast repetition rate techniques: defining methodology and experimental protocols. *Biochim biophys acta* **1367**(1–3), 88–106 (1998).
57. Oxborough, K. *et al.* Direct estimation of functional PSII reaction center concentration and PSII electron flux on a volume basis: a new approach to the analysis of Fast Repetition Rate fluorometry (FRRf) data. *Limnol Oceanogr: Methods* **10**(3), 142–154 (2012).
58. Sturn, A., Quackenbush, J. & Trajanoski, Z. Genesis: cluster analysis of microarray data. *Bioinformatics* **18**, 207–208 (2002).

Acknowledgements

The authors acknowledge the Swiss National Science Foundation for financial support (contract n° 205321_138254 and 200020_157173), Drs. Docquier and Barraclough (Genomics Platform, University of Geneva) for RNA-seq and transcriptome alignment, Mss. Moisset and Blanco Ameijeiras for helping with FRRf and Turner measurements, Dr Le Faucheur and Ms Dranguet for helping with WHAM calculations and Clive Prestt for English revision.

Author Contributions

R.B.-F., V.I.S., C.C. designed research; R.B.-F. performed research; R.B.-F., V.I.S., C.C. analyzed data and wrote the paper.

Additional Information

Supplementary information accompanies this paper at doi:[10.1038/s41598-017-08515-8](https://doi.org/10.1038/s41598-017-08515-8)

Competing Interests: The authors declare that they have no competing interests.

Publisher's note: Springer Nature remains neutral with regard to jurisdictional claims in published maps and institutional affiliations.



Open Access This article is licensed under a Creative Commons Attribution 4.0 International License, which permits use, sharing, adaptation, distribution and reproduction in any medium or format, as long as you give appropriate credit to the original author(s) and the source, provide a link to the Creative Commons license, and indicate if changes were made. The images or other third party material in this article are included in the article's Creative Commons license, unless indicated otherwise in a credit line to the material. If material is not included in the article's Creative Commons license and your intended use is not permitted by statutory regulation or exceeds the permitted use, you will need to obtain permission directly from the copyright holder. To view a copy of this license, visit <http://creativecommons.org/licenses/by/4.0/>.

© The Author(s) 2017